Earth and Planetary Science Letters 382 (2013) 58–65

Contents lists available at ScienceDirect

Earth and Planetary Science Letters

www.elsevier.com/locate/epsl

Quantifying magnetite magnetofossil contributions to sedimentary magnetizations

David Heslop [a,*], Andrew P. Roberts [a], Liao Chang [a,b], Maureen Davies [a], Alexandra Abrajevitch [a], Patrick De Deckker [a]

[a] Research School of Earth Sciences, The Australian National University, Canberra, ACT 0200, Australia
[b] Paleomagnetic Laboratory 'Fort Hoofddijk', Department of Earth Sciences, University of Utrecht, 3584 CD Utrecht, Netherlands

ARTICLE INFO

Article history:
Received 2 May 2013
Received in revised form 30 August 2013
Accepted 10 September 2013
Available online xxxx
Editor: J. Lynch-Stieglitz

Keywords:
natural remanent magnetization
magnetofossil
biogenic magnetite
Western Australia
Brunhes chron

ABSTRACT

Under suitable conditions, magnetofossils (the inorganic remains of magnetotactic bacteria) can contribute to the natural remanent magnetization (NRM) of sediments. In recent years, magnetofossils have been shown to be preserved commonly in marine sediments, which makes it essential to quantify their importance in palaeomagnetic recording. In this study, we examine a deep-sea sediment core from offshore of northwestern Western Australia. The magnetic mineral assemblage is dominated by continental detritus and magnetite magnetofossils. By separating magnetofossil and detrital components based on their different demagnetization characteristics, it is possible to quantify their respective contributions to the sedimentary NRM throughout the Brunhes chron. In the studied core, the contribution of magnetofossils to the NRM is controlled by large-scale climate changes, with their relative importance increasing during glacial periods when detrital inputs were low. Our results demonstrate that magnetite magnetofossils can dominate sedimentary NRMs in settings where they are preserved in significant abundances.

1. Introduction

Magnetotactic bacterial magnetosomes are permanent nanomagnets that, when arranged in chains, provide a means for the bacteria to orient themselves using Earth's magnetic field (Blakemore, 1975; Blakemore et al., 1980; Kirschvink, 1980a; Simmons et al., 2006). After death, these magnetically ideal single domain (SD) magnetosomes can be incorporated into the sedimentary matrix as magnetofossils. They then have the potential to contribute to sedimentary magnetizations if they maintain an existing alignment (or become aligned after burial) with the ambient geomagnetic field (Kirschvink, 1979; Stolz et al., 1986; Tarduno et al., 1998; Abrajevitch and Kodama, 2009) and if they avoid diagenetic dissolution through burial in anoxic environments (Karlin and Levi, 1983; Canfield and Berner, 1987). Their ideal SD size means that such magnetofossil-based magnetizations should provide a stable, but potentially nonlinear, record of geomagnetic field variations (Tauxe, 1993; Roberts et al., 2012).

Early studies identified magnetofossils in marine sediments and demonstrated that both chains and dispersed particles could carry stable laboratory-induced remanences (Kirschvink and Chang, 1984; Petersen et al., 1986; Stolz et al., 1986; Hesse, 1994). In some sediments, specific magnetofossil-rich horizons have elevated natural remanent magnetization (NRM) intensities with SD-like demagnetization characteristics, which suggests that magnetofossils contribute to their palaeomagnetic record (Tarduno et al., 1998; Abrajevitch and Kodama, 2009). These observations have led to the hypothesis that a biogeochemical remanent magnetization (BgRM), acquired by geomagnetically-aligned magnetosome chains preserving their orientation in the sedimentary record, can contribute to sedimentary NRMs. The consequences of BgRM acquisition would be especially important if the bacteria lived below the surface mixed sediment layer (e.g., Tarduno et al., 1998) and produced an NRM contribution that is offset from the palaeomagnetic signal carried by detrital particles. Alternatively, if magnetotactic bacteria lived in the water column or uppermost part of the sediment column, the post-mortem magnetofossil remains would be reoriented by both geomagnetic torques and a variety of sedimentary processes in the same manner as detrital magnetic particles. These magnetofossils would therefore contribute to a depositional (or postdepositional) remanent magnetization rather than a BgRM.

Testing the contribution of magnetofossils to the palaeomagnetic record has been a challenge until recently because of a lack of rock magnetic techniques that could be used to detect magnetofossils effectively. Instead, time-consuming magnetic extractions and transmission electron microscope (TEM) imaging were necessary to identify magnetofossil particles (e.g., Petersen et al., 1986; Hesse, 1994), which limits the number of samples that can be investigated.

* Corresponding author.

0012-821X/$ – see front matter
http://dx.doi.org/10.1016/j.epsl.2013.09.011

Developments in magnetic "remote sensing" have revealed that magnetofossils are much more widespread in the geological record than was thought previously (Egli, 2004; Egli et al., 2010; Roberts et al., 2012). Mathematical unmixing of laboratory-induced remanence curves demonstrates that a variety of sediment types contain apparent magnetofossil components with narrow size distributions and coercivities consistent with magnetite (Kruiver et al., 2001; Egli, 2004; Abrajevitch and Kodama, 2009). First-order reversal curve (FORC) measurements provide a joint measure of the coercivity and interaction field distribution for fine magnetic particle systems (Pike et al., 1999). Thus, FORC diagrams have high diagnostic power, and allow identification of different domain states of particles within mixed magnetic mineral assemblages (Roberts et al., 2000). FORC distributions from magnetosome chains have a clear SD signature with a wide distribution of coercivities, but minimal interactions (Pan et al., 2005; Chen et al., 2007; Carvallo et al., 2009; Roberts et al., 2012; Li et al., 2012). Egli et al. (2010) developed a high-resolution FORC measurement protocol that allows proper quantification of the distribution produced by non-interacting SD particles, the so-called "central ridge" in a FORC diagram. Magnetosomes are flux linked and in combination behave as a single elongated SD particle (Dunin-Borkowski et al., 1998; Muxworthy and Williams, 2006, 2009), so that intact magnetofossil chains will contribute to the FORC central ridge signature. High-resolution FORC distributions are, therefore, an important diagnostic tool for detecting magnetofossils.

While rock magnetic data can provide strong evidence for the presence of magnetofossils, their interpretation is not unique. TEM observations can support the presence of magnetofossils, which have specific compositions, crystal structures, a limited size spectrum and a restricted range of characteristic morphologies (Petersen et al., 1986; Tarduno et al., 1998; Kopp and Kirschvink, 2008). Although magnetic particle extraction and TEM imaging are time consuming, analysis of a small number of samples can provide sufficient evidence to interpret more rapidly acquired rock magnetic data in terms of magnetofossil identification. Using a combination of TEM and rock magnetic techniques, recent work has provided strong support for the common occurrence of magnetofossils in a variety of marine sediments (Roberts et al., 2011, 2012; Chang et al., 2012; Larrasoaña et al., 2012; Yamazaki, 2012; Yamazaki and Ikehara, 2012).

Now that the experimental tools needed to identify magnetofossils are available, it is important to quantify their contribution to sedimentary NRMs. In this study, we present results from a Quaternary marine sediment core in which magnetofossils appear to be ubiquitous and where their relative contribution to the NRM is primarily modulated by detrital input from the nearby Australian continent. When the relative magnetofossil abundance is high, the sedimentary magnetization becomes more SD-like in its characteristics, therefore providing strong support for a dominant contribution of magnetofossils to the NRM. With the assumption of a two end-member mixing system, the magnetofossil contribution to the overall sedimentary NRM can be determined as a function of age.

2. Geological setting

Core MD00-2361 (113°28.63′E, 22°04.92′S) was recovered ~41 km off the coast of northwestern Western Australia at a water depth of 1805 m during the *Marion Dufresne* TIP 2000 expedition (Fig. 1). The summer climate of this region is dominated by the Australian monsoon, with large rainfall episodes causing rivers to flood and transport large volumes of sediment to the ocean (Gingele et al., 2001a). Satellite images have revealed sediment-laden river plumes extending 200–300 km offshore during the northern Australia wet season (Gingele and De Deckker, 2004). The position of core MD00-2361 is ~160 km from the mouth of the Ashburton River (Fig. 1), in a location expected to receive suspended riverine sediment advected southward by the Leeuwin Current (Spooner et al., 2011, Fig. 1). During the winter months, northwestern Western Australia is dry and the rivers have a reduced carrying capacity, or in some cases they dry out completely (Gingele et al., 2001a). During such dry periods aeolian dust is transported eastward along the so-called Indian Ocean dust path and contributes to the terrigenous flux that reaches the Indian Ocean (Bowler, 1976; McTainsh, 1989; Hesse and McTainsh, 2003). The relative contributions of riverine and aeolian sediment fluxes that reach the Indian Ocean from northwestern Western Australia have been shown to vary on glacial–interglacial time scales. During glacial periods, northwestern Western Australia was relatively cold and arid, with increased aeolian fluxes and reduced riverine fluxes (Hesse, 1997, 2003). In contrast, interglacial periods were characterized by warm and wet conditions with increased river transport and reduced aeolian activity (Gingele et al., 2001b).

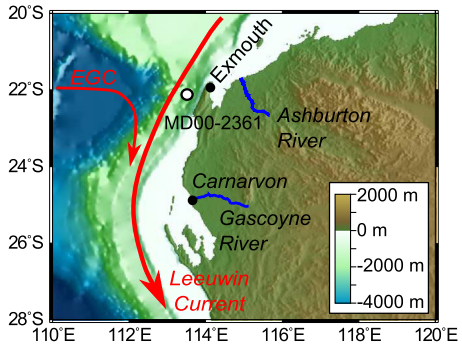

Fig. 1. Indian Ocean bathymetry and location of sediment core MD00-2361 (open symbol) offshore of northwestern Western Australia. The near-surface Eastern Gyral Current (EGC) and Leeuwin Current (red arrows) are adapted from Tomczak and Godfrey (1994). (For interpretation of the references to color in this figure legend, the reader is referred to the web version of this article.)

3. Materials and methods

Core MD00-2361 is 42 m long; we have analyzed the uppermost 16.5 m of the core in this study. We analyzed 11 continuous 1.5-m long u-channel samples from the upper portion of the core. A detailed late Quaternary palaeoceanographic reconstruction, based on the upper 13.6 m of core MD00-2361, has been published by Spooner et al. (2011).

Magnetic measurements were made at 1-cm intervals with a 2-G Enterprises narrow-access pass-through cryogenic magnetometer (Weeks et al., 1993) at the National Oceanography Centre, Southampton, UK. NRMs were demagnetized in 12 steps up to a maximum field of 100 mT with an alternating field (AF) demagnetizer that is arranged in-line with the magnetometer. NRM demagnetization data were analyzed with the UPmag software of Xuan and Channell (2009) and characteristic remanent magnetization (ChRM) directions were defined using the principal component analysis approach of Kirschvink (1980b). Isothermal remanent magnetizations (IRMs) were imparted to the u-channel samples with a 2-G Enterprises off-line pulse magnetizer. The IRM at 900 mT is assumed to represent the saturation isothermal remanent magnetization (SIRM).

Subsamples were taken from the u-channels at 10 cm stratigraphic intervals, and were crushed gently and air-dried. Hysteresis and backfield demagnetization measurements were performed using a Princeton Measurements Corporation vibrating sample magnetometer at the Research School of Earth Sciences, Australian National University. First-order reversal curve (FORC) diagrams (Pike et al., 1999; Roberts et al., 2000) were measured for a selection

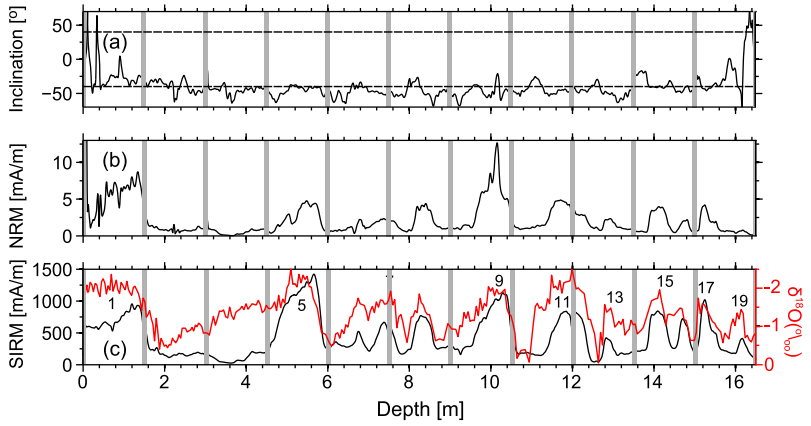

Fig. 2. (a) ChRM inclinations for the uppermost 16.5 m of sediment core MD00-2361. Vertical grey lines mark breaks between u-channel samples (at each break ±5 cm of data was removed to minimize edge effects). Horizontal dashed lines indicate the expected geocentric axial dipole inclinations for normal and reversed polarity fields at the site latitude. (b) NRM intensity plotted as a function of depth through core MD00-2361. (c) SIRM intensity (black) and planktonic δ^{18}O (red). The large-scale structure of the δ^{18}O record allows marine oxygen isotope stages to be assigned throughout the studied interval. For clarity, only interglacial periods (odd-numbered stages) are marked. (For interpretation of the references to color in this figure legend, the reader is referred to the web version of this article.)

of samples to investigate magnetic particle domain state and magnetostatic interactions. High-resolution FORC diagrams were measured with a field increment suitable for processing with a maximum smoothing factor (SF) of 5 and to enable robust identification of the central ridge feature associated with non-interacting SD particles (Egli et al., 2010). To improve FORC signal-to-noise ratios, magnetically weak samples were measured multiple times (maximum of 18 repetitions) and the FORC distributions were averaged. Statistically significant regions of the resulting FORC distributions were identified using the technique of Heslop and Roberts (2012a).

Zero-field cycling of a 2.5 T SIRM from 300 K to 10 K and back to 300 K was performed on a small number of subsamples. This measurement procedure provides information concerning both the Verwey transition and the degree of oxidation of magnetite particles (Özdemir and Dunlop, 2010). Low temperature measurements were performed using a Quantum Design Magnetic Properties Measurement System (MPMS) housed at the Research School of Earth Sciences, Australian National University.

Magnetic particles were extracted for TEM analysis using the procedure of Chang et al. (2012). Magnetic extracts were imaged using a Philips CM300 TEM operated at 300 kV at the Research School of Earth Sciences, Australian National University. The TEM has an EDAX Phoenix retractable X-ray detector and a Gatan 1024 × 1024 CCD camera.

Spooner et al. (2011) published a planktonic oxygen isotope stratigraphy for the upper 13.6 m of core MD00-2361. For this study their oxygen isotope record was extended to 16.5 m using the same approach and mass spectrometer as described by Spooner et al. (2011). Additional measurements were also made where the original sampling resolution of Spooner et al. (2011) was comparatively low.

4. Results

ChRM inclinations through the majority of the studied interval of core MD00-2361 lie around the direction expected for a normal polarity geocentric axial dipole field (Fig. 2a). At a depth of ∼16.2 m there is a clear transition from reversed to normal polarity. A coherent ChRM inclination pattern is not observed in the uppermost ∼0.5 m of core MD00-2361 probably due to disturbance of unconsolidated sediments during coring. The fluctuating signal observed in this portion of the core is not considered to provide a reliable record of geomagnetic field variations. NRM intensities (Fig. 2b) follow a similar pattern to SIRM variations (Fig. 2c). This demonstrates that the primary control on the NRM intensity is the concentration and composition of magnetic minerals in the sediment rather than palaeomagnetic field strength.

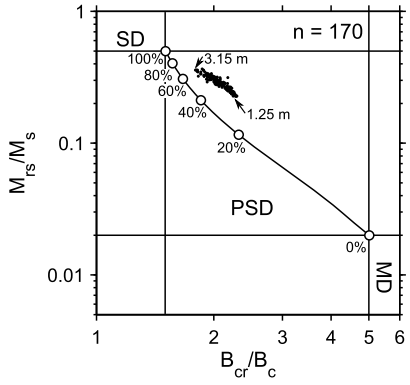

Fig. 3. Day plot (cf., Day et al., 1977) for the 170 subsamples analyzed from MD00-2361. The data are bunched tightly in the PSD field and are located to the right of the mixing line of Dunlop (2002a) for SD + MD magnetite. Numbers next to the mixing line indicate the volumetric fraction of SD particles. Based on the data distribution, samples from 1.25 and 3.15 m were selected for further analysis and correspond to the coarsest (interglacial) and finest (glacial) magnetic particle assemblages, respectively.

Comparison of the supplemented and extended planktonic oxygen isotope stratigraphy for core MD00-2361 with SIRM (Fig. 2c) reveals a low frequency variability that is consistent with that expected for glacial–interglacial cyclicity (Lisiecki and Raymo, 2005). Based on the large-scale oxygen isotope pattern, marine isotope stages can be assigned for core MD00-2361. On the basis of the oxygen isotope stratigraphy for core MD00-2361, the magnetic reversal at ∼16.2 m occurs within marine isotope stage (MIS) 19 and must correspond to the Matuyama–Brunhes boundary (Tauxe et al., 1996; Liu et al., 2008), thus the base of the studied sediment sequence is dated at ∼800 ka (corresponding to a mean sedimentation rate of ∼2 cm/kyr).

Hysteresis ratios for samples from core MD00-2361 lie within the pseudo-single domain (PSD) field in a Day plot (cf. Day et al., 1977, Fig. 3). Using an SD versus multidomain (MD) binary mixing line as a general guide (Dunlop, 2002a, 2002b), it appears that the sediments contain a mixture of SD and coarser grains. On the basis of the Day plot, glacial sediments at 3.15 m contain the finest overall magnetic mineral assemblage. A high content of non-interacting SD particles is confirmed at 3.15 m by a statistically significant central ridge in the high-resolution FORC distribution

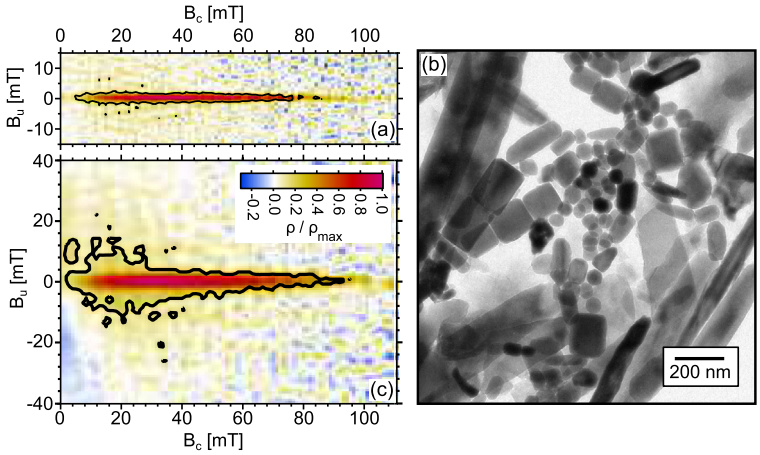

Fig. 4. (a) High-resolution FORC distribution (smoothing factor of 5) for glacial sediments from 3.15 m in core MD00-2361 (the black contour is the 0.05 significance level). The final high-resolution FORC diagram was obtained by stacking 18 measured FORC diagrams, each constructed from 297 FORCs. The sharp central ridge that dominates the diagram is indicative of non-interacting SD particles that reflect the presence of magnetite magnetofossils (Egli et al., 2010; Roberts et al., 2012). (b) TEM image of a magnetic mineral extract from 3.15 m. The image is dominated by magnetite magnetofossils with a variety of morphologies (the larger particles are non-magnetic contaminants, such as carbonates and clays). (c) Low-resolution FORC distribution (207 FORCs, smoothing factor of 5, with 18 repeat measurements stacked) from the same sediment sample with slight vertical spreading at low coercivities. This spread is most likely due to the presence of a minor coarse-grained detrital component.

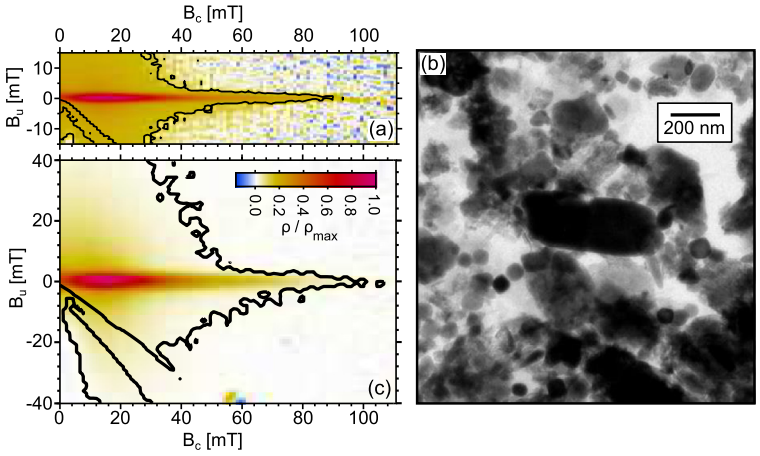

Fig. 5. (a) High-resolution FORC distribution (smoothing factor of 5) for interglacial sediments from 1.25 m (the black contour is the 0.05 significance level). This FORC diagram was obtained by stacking 8 measured FORC diagrams, each constructed from 297 FORCs. The combination of a sharp central ridge and large vertical spread indicates a mixed magnetic mineral assemblage with SD particles and coarser PSD/MD grains. The break in the region of significant values at negative B_u values results from the inability of a second-order polynomial surface to fit the data across $B = 0$ (Egli, 2013). (b) TEM image of a magnetic extract from 1.25 m with large detrital particles and smaller magnetofossils, which is consistent with the interpretation of the associated FORC distributions. (c) Low-resolution FORC distribution (207 FORCs, smoothing factor of 5, stack of 4 repeat measurements) from the same sample, which confirms the structure of the high-resolution distribution.

(Fig. 4a). While a central ridge FORC signature is characteristic of magnetofossils it is not necessarily an unequivocal indicator of biogenic magnetite particles. TEM images of magnetic mineral extracts taken at 3.15 m demonstrate that the magnetic mineral assemblage is dominated by magnetofossils, both as discrete particles and as apparently collapsed and intact chains (Fig. 4b). The generally disaggregated or collapsed nature of magnetofossil chains is probably the result of the sample preparation procedure required to extract magnetic minerals from bulk sediment samples. Energy dispersive X-ray spectra analysis and selected-area electron diffraction performed on individual particles confirm a magnetite composition. The crystal morphology is also as expected for biogenic magnetite particles. Lower resolution FORC distributions place less emphasis on the central ridge and may reveal contributions from larger particles and magnetostatic interactions among particles. The lower resolution FORC distribution for the sample from 3.15 m has a slightly broadened central ridge at low B_c values (Fig. 4c). This broadening could be due to collapsed chains, but given the depositional setting it is more likely to correspond to a minor contribution from coarser detrital (PSD and/or MD) grains.

In the Day plot, the coarsest overall magnetic mineral assemblages are found in interglacial sediments (Fig. 3). The sediments at 1.25 m are early Holocene in age and a high-resolution FORC distribution contains both a central ridge and significant vertical spreading (Fig. 5a). This combination of features indicates a mixed magnetic mineral assemblage containing both non-interacting SD particles and a substantial contribution from coarser PSD/MD grains (Roberts et al., 2000). TEM images of a magnetic mineral extract from a sample at 1.25 m support our interpretation that the FORC distribution reflects a mixture of magnetofossils and larger particles (Fig. 5b), as is also by the lower resolution FORC distribution, which has an essentially identical structure to the high-resolution distribution (Fig. 5c).

Zero-field cycling of a 2.5 T SIRM was performed on the subsamples from 1.25 m and 3.15 m (Fig. 6). The Verwey transition is apparent in both samples (although it is more pronounced for the sample from 3.15 m), which supports the TEM and FORC evidence for the presence of magnetite magnetofossils in core MD00-2361. The weak nature of the Verwey transition in both samples does, however, indicate that the magnetofossils may be partially oxidized

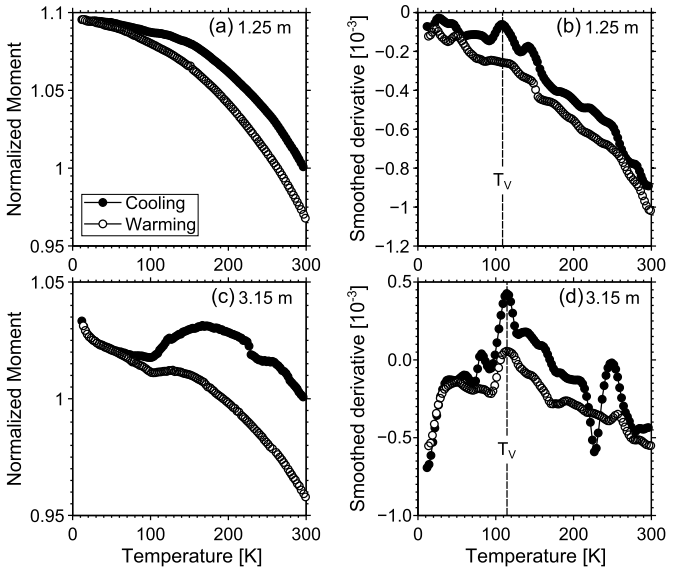

Fig. 6. (a) Zero-field cycling from 300 K to 10 K and back to 300 K for a 2.5 T SIRM from an interglacial sediment sample taken at 1.25 m. (b) Derivatives of the cooling and warming curves shown in (a) calculated with a smoothing spline (de Boor, 1994). The overall structure of the cycling is indicative of oxidized magnetite with the cooling curve containing a strongly suppressed Verwey transition (marked as T_V). (c) Zero-field cycling of a 2.5 T SIRM from a glacial sediment sample taken at 3.15 m. This sample is relatively enriched in magnetofossils and exhibits a clearer Verwey transition as demonstrated by the smoothed derivatives in (d).

(Moskowitz et al., 1993; Smirnov and Tarduno, 2000; Kopp et al., 2006), which is common in sediments. The generally increasing remanence as a function of decreasing temperature and limited loss of remanence during cycling demonstrates that in addition to magnetite magnetofossils the magnetic mineral assemblage contains an oxidized magnetite component (Özdemir and Dunlop, 2010).

Measurement data from this study can be accessed online via PANGAEA (http://www.pangaea.de/).

5. Discussion

Comparison of the SIRM and planktonic oxygen isotope records from core MD00-2361 demonstrates a clear climatic control over the magnetic mineral assemblage (Fig. 2c). Studies covering shorter time scales have shown that during interglacial periods, precipitation increased over northwestern Western Australia and a greater riverine sediment load reached the MD00-2361 site (Veeh et al., 2000; Gingele et al., 2001b; van der Kaars and De Deckker, 2002). This process is illustrated in the studied sediment core by the presence of pigmenting riverine clays during each interglacial interval (Gingele et al., 2001b; Gingele and De Deckker, 2004; Spooner et al., 2011). The rivers that flow into the Indian Ocean from northwestern Australia have brown colored water because they transport fine-grained material that originates inland from iron-rich regolith. Sediments corresponding to MIS 1, 5, 7 and 9 have a (chocolate) brown color, while sediments deposited during MIS 11, 13, 15, 17 and 19 are a lighter beige color, which suggests a relative shift to greater riverine fluxes in more recent times. Given the elevated SIRM values during interglacial periods, this detrital material must be relatively enriched in magnetic minerals. The opposite situation occurred during glacial periods, with reduced precipitation and a lower detrital mineral flux resulting in diminished SIRM values. If aeolian dust was reaching the location of core MD00-2361 during glacials, the low SIRM values observed during these periods indicate that the contribution of aeolian magnetic

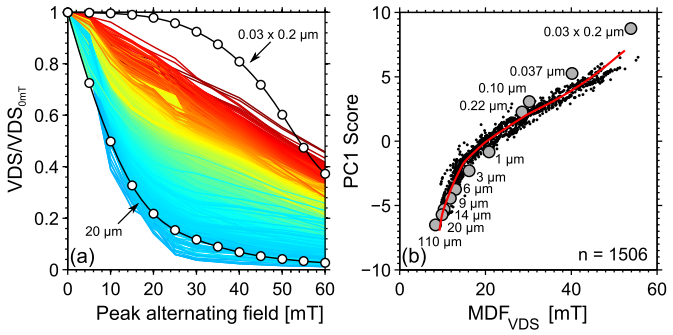

Fig. 7. (a) Normalized vector difference sum (VDS) AF demagnetization curves for the 0.5–16.5 m depth interval for core MD00-2361 (1506 curves). For clarity, the curves are color-coded according to their MDF (blue and red correspond to soft and hard, respectively). For comparison the AF demagnetization curves are shown for sized magnetites carrying a TRM imparted in a 0.1 mT direct field (Dunlop and Özdemir, 1997). (b) The trajectory (red line) of the first VDS principal component as a function of MDF. Individual VDS curves (black dots) from core MD00-2361 follow the principal component closely, which suggests that the sedimentary NRM comprises a two-component linear mixing system. The AF demagnetization curves for sized TRM-bearing magnetites are projected onto the same principal component (grey points with particle sizes marked) and correspond closely with the sedimentary data from core MD00-2361. (For interpretation of the references to color in this figure legend, the reader is referred to the web version of this article.)

particles to the sedimentary NRM (i.e., particles in the stable SD to MD range) was minor.

A scenario in which the magnetic properties of the sediments are dominated by magnetofossils and riverine detritus during glacial and interglacial periods, respectively, is consistent with hysteresis, TEM, FORC and low temperature data presented in Figs. 3, 4, 5 and 6. Sediments from 1.25 m (interglacial) contain a mixture of SD magnetofossils and coarser PSD/MD riverine particles, while sediments from 3.15 m (glacial) are rich in magnetofossils with only a minor detrital magnetic mineral concentration. The low temperature cycling data support this interpretation with a more predominant Verwey transition at 3.15 m (glacial sediments) compared to 1.25 m (interglacial sediments). This two end-member mixing system, with an alternating pattern of glacial (relatively magnetofossil-rich/detritus-poor) and interglacial (relatively magnetofossil-poor/detritus-rich) sediments, allows quantification of the contribution of magnetofossils to the sedimentary NRM.

In fine magnetic particle systems many magnetic properties are a function of grain size. These properties thus provide a means with which to investigate magnetic mineral assemblages that contain a mixture of different particle sizes. AF demagnetization curves for a thermoremanent magnetization (TRM) in magnetite depend strongly on grain size (see the results of Argyle et al., 1994 as presented by Dunlop and Özdemir, 1997). Larger particles are magnetically soft and give rise to concave-up demagnetization curves, while finer particles are magnetically harder so that SD sizes produce sigmoidal demagnetization curves. Detrital particles in a sediment produce a depositional remanent magnetization (DRM), however, individually they carry a TRM or chemical remanent magnetization (CRM) from the time of their formation. In a similar manner, individual magnetofossils will contribute to the NRM, but they will carry individual CRMs that formed when they grew through their blocking volume and acquired a stable SD magnetization. Magnetite TRMs and CRMs have similar AF demagnetization spectra (Kobayashi, 1959), which allows the NRM contributions carried by magnetofossils and detrital particles to be compared directly.

To assess the relative contribution of magnetofossils and detrital particles to the NRM of core MD00-2361 the vector difference sum (VDS, Gee et al., 1993) of each NRM demagnetization curve was calculated. This involves summing the magnetization vector

differences for a given sample at each AF demagnetization step to provide a representation of the total NRM demagnetization curve rather than the measured resultant curve, which may contain cancellation of non-aligned components. The 1506 normalized (i.e., $VDS/VDS_{0\,mT}$) demagnetization curves from core MD00-2361 are shown in Fig. 7a. The observed spectrum of patterns range from strongly concave up, which is indicative of an NRM carried by coarse grains, to almost straight lines, which are hypothesized to be a mixture of fine (magnetofossil) and coarse (detrital) particles.

To test the hypothesis that the NRM in core MD00-2361 is carried by both magnetofossils and detrital particles, we performed a principal component analysis on the normalized VDS demagnetization curves. VDS magnetizations at a given AF demagnetization step were standardized (zero mean and unit standard deviation) to produce a centered 10-dimensional data distribution. The principal component solution through this multivariate space was then calculated using singular value decomposition (Jolliffe, 2002). Over 89% of the standardized VDS variance is explained by the first principal component (i.e., the leading eigenvector through the centered data), which provides strong support for the presence of a two-component linear mixing system (Heslop and Roberts, 2012b). There is a clear relationship between the position of each VDS curve on the first principal component (represented by the so-called *score*) and the median destructive field (MDF) of that curve (Fig. 7b). This demonstrates that the principal component is controlled by the shape of the VDS curves. For comparison the AF demagnetization curves for sized magnetites with a TRM imparted in a 0.1 mT direct field (Argyle et al., 1994) were projected onto the first VDS principal component (Fig. 7b). As a function of MDF, the VDS for core MD00-2631 and magnetite TRMs follow slightly different paths, however, there is good correspondence in terms of overlap and trend of the two data sets. Although the first principal component defines an empirical binary mixing line through the VDS data, the locations of the two end-members on the mixing line are unknown. While it is possible to define arbitrary points to act as end-members, for example, the extremes of the data, we have used prior information to define end-members that are consistent with the rock magnetic and TEM analyses presented in Section 4.

While the TRM experiments of Argyle et al. (1994) demonstrate that magnetite demagnetization curves change their form as a function of particle size, the geological setting of core MD00-2361 and mineral magnetic data from this core imply that the VDS curves are a function of the relative NRM contributions of fine SD magnetofossils and coarse PSD/MD detrital particles. To estimate their relative contributions, TRM demagnetization curves for 0.03×0.2 μm and 20 μm particles (Fig. 7a) were selected as end-members on the basis of the distribution of the TRM and demagnetization curves for core MD00-2361 along the first VDS principal component (Fig. 7b). Thus, the end-member model assumes that the 0.03×0.2 μm and 20 μm TRM demagnetization curves represent the VDS demagnetization of the magnetofossil and detrital components, respectively, for core MD00-2361. It is important to note that for magnetite grain sizes greater than ~10 μm, TRM demagnetization curves are highly similar (Argyle et al., 1994). Therefore, the end-member model will be relatively insensitive to the assumed particle size of the detrital end-member. Additionally, as a result of the geological age and heavy weathering of the northwestern Western Australian hinterland, the riverine flux reaching the Indian Ocean is thought to have maintained a practically constant composition on glacial–interglacial time scales (Gingele et al., 2001b). It is possible that the detrital component contains an SD contribution that would be mistakenly quantified as magnetofossils during the unmixing process. The effects of such misidentification are, however, expected to be minor given that the magnetic mineral assemblage of the riverine flux is dominated by coarse-grained particles.

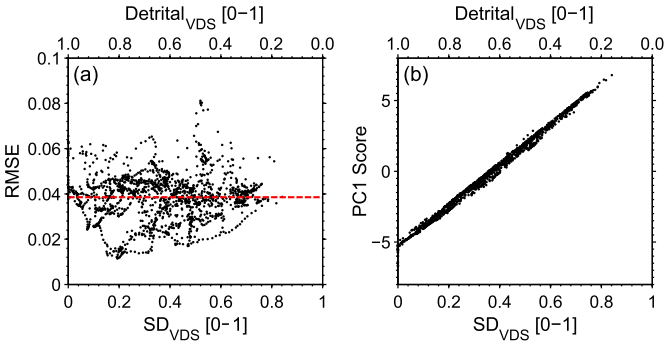

Fig. 8. (a) Dimensionless root mean squared error (RMSE) of the estimated end-member fit to each normalized VDS curve as a function of the relative contribution of the selected SD magnetofossil and detrital end-members. The dashed line marks the average fitting error across the entire normalized data set, which corresponds to an average RMSE below 0.04. (b) Relative contributions of the SD magnetofossil and detrital end-members to the total sediment VDS compared to the first principal component score of each VDS curve.

Relative contributions of the two magnetite TRM end-members to each normalized VDS curve for core MD00-2361 were estimated using constrained non-negative least squares (Lawson and Hanson, 1974). Additionally, the field steps on each curve were bootstrapped 1000 times with replacement (i.e., any given field step could be selected more than once in a given bootstrap sample) to provide a numerical assessment of the uncertainties on the estimated relative contributions (Efron and Tibshirani, 1993). The fitting errors between the VDS curves and their representation in the end-member mixing model are shown in Fig. 8a. Across the entire normalized VDS data set the average root mean squared error corresponds to a misfit between the demagnetization curves and the mixing model of <0.04. The estimated relative contributions have a tight linear relationship with the first principal component scores of the normalized VDS curves (Fig. 8b). This indicates a close correspondence between the empirical binary mixing line defined by the first principal component and our supervised unmixing model based on prior knowledge of the end-member compositions.

The relative down-core contribution of the SD end-member has a pattern consistent with the changing grain size of the magnetic mineral assemblage on glacial–interglacial timescales (Fig. 9). During interglacials, the NRM is dominated by a coarse-grained contribution carried by the riverine detrital component. In contrast, during glacials, when the detrital mineral flux was low, the NRM is dominated (up to ~80%) by an SD-like component, which FORC and TEM analyses indicate to be due to magnetite magnetofossils. This demonstrates that, under appropriate conditions, magnetofossils can make a dominant contribution to the total sedimentary NRM. If the detrital and magnetofossil components acquired their respective NRM contributions at different depths with respect to the sediment–water interface, then it is possible that the two NRM components for any given depth in the core were acquired in different fields. Such a process would bias the unmixing results toward an over-representation of whichever component formed in the stronger field. However, given that the overall pattern of NRM contributions is consistent with the climatically controlled abundances of fluvial and biogenic magnetic particles, it must be concluded that the palaeomagnetic field could only have played a minor role in controlling the relative contributions of the two components to the sedimentary NRM.

The presented unmixing analysis employs normalized VDS and TRM demagnetization curves to provide estimates of the relative contribution of SD magnetofossils to the total sediment VDS (Fig. 9). Because of the different grain sizes of the detrital

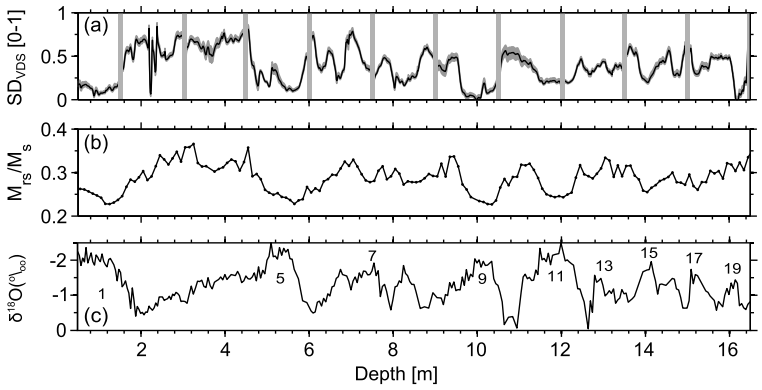

Fig. 9. (a) Relative contribution of SD magnetofossils to the total sediment VDS (vertical grey lines mark breaks between u-channel samples). The black line represents the median contribution determined from 1000 bootstrap iterations and the 95% confidence interval is indicated by shading about the line. (b) Variation in the grain-size-indicative hysteresis ratio M_{rs}/M_s, which indicates that the sediments with fine magnetic particle assemblages carry a relatively larger NRM contribution from SD magnetofossils. (c) Planktonic δ^{18}O record, with clear glacial–interglacial stratigraphy, for core MD00-2361 (for clarity, only interglacial periods are numbered).

and biogenic end-members, however, it is not possible to use component-specific relative palaeointensity parameters, such as NRM/IRM, to determine the relative efficiencies with which the two components acquired their NRM. Lowrie and Fuller (1971) demonstrated that AF demagnetization curves for TRMs and IRMs have different relationships for SD and MD particles. Thus, NRM/IRM for a given component will provide only a compounded representation of both NRM acquisition efficiency and grain size. Additionally, the large glacial–interglacial changes in magnetic mineral concentration mean that the studied sediments are not sufficiently uniform to be suitable for relative palaeointensity analysis (see, Tauxe, 1993).

6. Conclusions

We have analyzed a sediment core from offshore of northwestern Western Australia in which the magnetic mineral assemblage is a climatically controlled two-component mixing system. During glacial periods, the magnetic mineral assemblage of core MD00-2361 is dominated by SD magnetite magnetofossils. Contrastingly, during interglacials, an increased riverine flux of coarse PSD/MD detritus reached the core site, which reduced the relative abundance of magnetofossils. By demarcating the magnetofossil and detrital particle contributions on the basis of their size-dependent demagnetization characteristics, it is possible to estimate the contribution of magnetofossils to the overall sediment NRM.

During glacial periods, the sediments in core MD00-2361 were relatively enriched in magnetofossils that dominate the NRM (reaching contributions as high as ~80%). Interglacial sediments are enriched in detrital minerals and in relative terms the magnetofossil contribution to the NRM decreases (typically below ~30%). While results from core MD00-2361 reveal a clear magnetofossil contribution to the NRM, it is not apparent whether the magnetic signal formed actively (i.e., via a BgRM mechanism with bacteria aligning with the field and chains remaining oriented after death) or passively (i.e. via a (post)depositional remanent magnetization with magnetofossils being reworked in the sediment post-mortem and aligning with the field). Whatever the remanence acquisition mechanism, magnetofossils have been shown to be widely preserved in the geological record in a range of sediment types (Roberts et al., 2012), which makes them a potentially important contributor to sediment magnetizations. Our approach provides a method with which to quantify magnetofossil contributions in future assessments of the extent to which biogeochemical remanent magnetizations may be important in the geological record.

Acknowledgements

We are grateful for constructive comments from three reviewers and the Editor. This work was supported by the Australian Research Council (grants DP110105419 and DP120103952). The authors thank Jan-Berend Stuut for his assistance in sampling the sediment core and the School of Ocean and Earth Science at the University of Southampton for providing access to the Palaeomagnetic Laboratory at the National Oceanography Centre, Southampton.

References

Abrajevitch, A., Kodama, K., 2009. Biochemical vs. detrital mechanism of remanence acquisition in marine carbonates: a lesson from the K-T boundary interval. Earth Planet. Sci. Lett. 286, 269–277.
Argyle, K.S., Dunlop, D.J., Xu, S., 1994. Single-domain behavior of multidomain magnetite grains (abstract). Eos 75, 196.
Blakemore, R.P., 1975. Magnetotactic bacteria. Science 190, 377–379.
Blakemore, R.P., Frankel, R.B., Kalmijn, A.J., 1980. South-seeking magnetotactic bacteria in the Southern Hemisphere. Science 286, 384–385.
Bowler, J.M., 1976. Aridity in Australia: age, origins and expressions in aeolian landforms and sediments. Earth-Sci. Rev. 12, 279–310.
Canfield, D.E., Berner, R.A., 1987. Dissolution and pyritization of magnetite in anoxic marine sediments. Geochim. Cosmochim. Acta 51, 645–659.
Carvallo, C., Hickey, S., Faivre, D., Menguy, N., 2009. Formation of magnetite in *Magnetospirillum gryphiwaldense* studied with FORC diagrams. Earth Planets Space 61, 143–150.
Chang, L., Roberts, A.P., Williams, W., Fitz Gerald, J.D., Larrasoaña, J.C., Jovane, L., Muxworthy, A.R., 2012. Giant magnetofossils and hyperthermal events. Earth Planet. Sci. Lett. 351–352, 258–269.
Chen, A.P., Egli, R., Moskowitz, B.M., 2007. First-order reversal curve (FORC) diagrams of natural and cultured biogenic magnetite particles. J. Geophys. Res. 112, B08S90, http://dx.doi.org/10.1029/2006JB004575.
Day, R., Fuller, M., Schmidt, V.A., 1977. Hysteresis properties of titanomagnetites: grain-size and compositional dependence. Phys. Earth Planet. Inter. 13, 260–267, http://dx.doi.org/10.1016/0031-9201(77)90108-X.
de Boor, C., 1994. A Practical Guide to Splines. Springer Verlag.
Dunin-Borkowski, R.E., McCartney, M.R., Frankel, R.B., Bazylinski, D.A., Pósfai, M., Buseck, P.R., 1998. Magnetic microstructure of magnetotactic bacteria by electron holography. Science 282, 1868–1870.
Dunlop, D.J., 2002a. Theory and application of the Day plot (M_{rs}/M_s versus H_{cr}/H_c) 1. Theoretical curves and tests using titanomagnetite data. J. Geophys. Res. 107 (B3), 2056, http://dx.doi.org/10.1029/2001JB000486.
Dunlop, D.J., 2002b. Theory and application of the Day plot (M_{rs}/M_s versus H_{cr}/H_c) 2. Application to data for rocks, sediments, and soils. J. Geophys. Res. 107 (B3), 2057, http://dx.doi.org/10.1029/2001JB000487.
Dunlop, D.J., Özdemir, Ö., 1997. Rock Magnetism: Fundamentals and Frontiers. Cambridge University Press, Cambridge, UK.
Efron, B., Tibshirani, R.J., 1993. An Introduction to the Bootstrap. Chapman & Hall, New York.
Egli, R., 2004. Characterization of individual rock magnetic components by analysis of remanence curves, 1. Unmixing natural sediments. Stud. Geophys. Geod. 48, 391–446.

Egli, R., 2013. VARIFORC: an optimized protocol for the calculation of non-regular first-order reversal curves (FORC) diagrams. Glob. Planet. Change, http://dx.doi.org/10.1016/j.gloplacha.2013.08.003, in press.

Egli, R., Chen, A.P., Winklhofer, M., Kodama, K.P., Horng, C.S., 2010. Detection of noninteracting single domain particles using first-order reversal curve diagrams. Geochem. Geophys. Geosyst. 11, Q01Z11, http://dx.doi.org/10.1029/2009GC002916.

Gee, J., Staudigel, H., Tauxe, L., Pick, T., Gallet, Y., 1993. Magnetization of the La Palma Seamount Series: implications for seamount paleopoles. J. Geophys. Res. 98, 11743–11767.

Gingele, F.X., De Deckker, P., 2004. Fingerprinting Australia's rivers with clay minerals and the application for the marine record of climate change. Aust. J. Earth Sci. 51, 339–348.

Gingele, F.X., De Deckker, P., Hillenbrand, C.D., 2001a. Clay mineral distribution in surface sediments between Indonesia and NW Australia – source and transport by ocean currents. Mar. Geol. 179, 135–146.

Gingele, F.X., De Deckker, P., Hillenbrand, C.D., 2001b. Late Quaternary fluctuations of the Leeuwin Current and palaeoclimates on the adjacent landmasses: clay mineral evidence. Aust. J. Earth Sci. 48, 867–874.

Heslop, D., Roberts, A.P., 2012a. Estimation of significance levels and confidence intervals for first-order reversal curve diagrams. Geochem. Geophys. Geosyst. 13, Q12Z40, http://dx.doi.org/10.1029/2012GC004115.

Heslop, D., Roberts, A.P., 2012b. Estimating best-fit binary mixing lines in the Day plot. J. Geophys. Res. 117, B01101, http://dx.doi.org/10.1029/2011JB008787.

Hesse, P.P., 1994. Evidence for bacterial palaeoecological origin of mineral magnetic cycles in oxic and sub-oxic Tasman Sea sediments. Mar. Geol. 117, 1–17.

Hesse, P.P., 1997. Mineral magnetic 'tracing' of aeolian dust in southwest Pacific sediments. Palaeogeogr. Palaeoclimatol. Palaeoecol. 131, 327–353.

Hesse, P.P., McTainsh, G.H., 2003. Australian dust deposits: modern processes and the Quaternary Record. Quat. Sci. Rev. 22, 2007–2035.

Jolliffe, I.T., 2002. Principal Component Analysis, 2nd ed. Cambridge University Press.

Karlin, R., Levi, S., 1983. Diagenesis of magnetic minerals in Recent haemipelagic sediments. Nature 303, 327–330.

Kirschvink, J.L., 1979. Mineralization and magnetization of chiton teeth: paleomagnetic, sedimentologic, and biological implications of organic magnetite. Earth Planet. Sci. Lett. 44, 193–204.

Kirschvink, J.L., 1980a. South-seeking magnetic bacteria. J. Exp. Biol. 86, 345–347.

Kirschvink, J.L., 1980b. The least-squares line and plane and the analysis of palaeomagnetic data. Geophys. J. R. Astron. Soc. 62, 699–718.

Kirschvink, J.L., Chang, S.R., 1984. Ultrafine-grained magnetite in deep-sea sediments: possible bacterial magnetofossils. Geology 12, 559–562.

Kobayashi, K., 1959. Chemical remanent magnetization of ferromagnetic minerals and its application to rock magnetism. J. Geomagn. Geoelectr. 10, 99–117.

Kopp, R.E., Kirschvink, J.L., 2008. The identification and biogeochemical interpretation of fossil magnetotactic bacteria. Earth Sci. Rev. 86, 42–61.

Kopp, R.E., Weiss, B.P., Maloof, A.C., Vali, H., Nash, C.Z., Kirschvink, J.L., 2006. Chains, clumps, and strings: magnetofossil taphonomy with ferromagnetic resonance spectroscopy. Earth Planet. Sci. Lett. 247, 10–25.

Kruiver, P.P., Dekkers, M.J., Heslop, D., 2001. Quantification of magnetic coercivity components by the analysis of acquisition curves of isothermal remanent magnetisation. Phys. Earth Planet. Inter. 189, 269–276.

Larrasoaña, J.C., Roberts, A.P., Chang, L., Schellenberg, S.A., Fitz Gerald, J.D., Norris, R.D., Zachos, J.C., 2012. Magnetotactic bacterial response to Antarctic dust supply during the Palaeocene–Eocene thermal maximum. Earth Planet. Sci. Lett. 333–334, 122–133.

Lawson, C.L., Hanson, R.J., 1974. Solving Least Squares Problems. Prentice-Hall.

Li, J., Wu, W., Liu, Q., Pan, Y., 2012. Magnetic anisotropy, magnetostatic interactions and identification of magnetofossils. Geochem. Geophys. Geosyst. 13, Q10Z51, http://dx.doi.org/10.1029/2012GC004384.

Lisiecki, L.E., Raymo, M.E., 2005. A Pliocene–Pleistocene stack of 57 globally distributed benthic δ^{18}O records. Paleoceanography 20, PA1003, http://dx.doi.org/10.1029/2004PA001071.

Liu, Q., Roberts, A.P., Rohling, E.J., Zhu, R., Sun, Y., 2008. Post-depositional remanent magnetization lock-in and the location of the Matuyama–Brunhes geomagnetic reversal boundary in marine and Chinese loess sequences. Earth Planet. Sci. Lett. 275, 102–110.

Lowrie, W., Fuller, M., 1971. On the alternating field demagnetization characteristics of multidomain thermoremanent magnetization in magnetite. J. Geophys. Res. 76, 6339–6349.

McTainsh, G.H., 1989. Quaternary aeolian dust processes and sediments in the Australian region. Quat. Sci. Rev. 8, 235–253.

Moskowitz, B.M., Frankel, R.B., Bazylinski, D.A., 1993. Rock magnetic criteria for the detection of biogenic magnetite. Earth Planet. Sci. Lett. 120, 283–300.

Muxworthy, A.R., Williams, W., 2006. Critical single-domain/multidomain grain sizes in noninteracting and interacting elongated magnetite particles: implications for magnetosomes. J. Geophys. Res. 11, B12S12, http://dx.doi.org/10.1029/2006JB004588.

Muxworthy, A.R., Williams, W., 2009. Critical superparamagnetic/single domain grain sizes in interacting magnetite particles: implications for magnetosome crystals. J. R. Soc. Interface 6, 1207–1212.

Özdemir, Ö., Dunlop, D., 2010. Hallmarks of maghemitization in low-temperature remanence cycling of partially oxidized magnetite nanoparticles. J. Geophys. Res. 115, B02101, http://dx.doi.org/10.1029/2009JB006756.

Pan, Y., Petersen, N., Winklhofer, M., Davila, A.F., Liu, Q., Frederichs, T., Hanzlik, M., Zhu, R., 2005. Rock magnetic properties of uncultured magnetotactic bacteria. Earth Planet. Sci. Lett. 237, 311–325, http://dx.doi.org/10.1016/j.epsl.2005.06.029.

Petersen, N., von Dobeneck T, Vali, H., 1986. Fossil bacterial magnetite in deep-sea sediments from the South Atlantic Ocean. Nature 320, 611–615.

Pike, C.R., Roberts, A.P., Verosub, K.L., 1999. Characterizing interactions in fine magnetic particle systems using first order reversal curves. J. Appl. Phys. 85, 6660–6667, http://dx.doi.org/10.1063/1.370176.

Roberts, A.P., Pike, C.R., Verosub, K.L., 2000. First-order reversal curve diagrams: a new tool for characterizing the magnetic properties of natural samples. J. Geophys. Res. 105, 28461–28475, http://dx.doi.org/10.1029/2000JB900326.

Roberts, A.P., Florindo, F., Villa, G., Chang, L., Jovane, L., Bohaty, S.M., Larrasoaña, J.C., Heslop, D., Fitz Gerald, J.D., 2011. Magnetotactic bacterial abundance in pelagic marine environments is limited by organic carbon flux and availability of dissolved iron. Earth Planet. Sci. Lett. 310, 441–452.

Roberts, A.P., Chang, L., Heslop, D., Florindo, F., Larrasoaña, J.C., 2012. Searching for single domain magnetite in the "pseudo-single-domain" sedimentary haystack: implications of biogenic magnetite preservation for sediment magnetism and relative paleointensity determinations. J. Geophys. Res. 117, B08104, http://dx.doi.org/10.1029/2012JB009412.

Simmons, S.L., Bazylinski, D.A., Edwards, K.J., 2006. South-seeking magnetotactic bacteria in the Northern Hemisphere. Science 311, 371–374.

Smirnov, A.V., Tarduno, J.A., 2000. Low-temperature magnetic properties of pelagic sediments (Ocean Drilling Program Site 805C): Tracers of maghemitization and magnetic mineral reduction. J. Geophys. Res. 105, 16457–16471.

Spooner, M.I., De Deckker, P., Barrows, T.T., Fifield, L.K., 2011. The behaviour of the Leeuwin Current offshore NW Australia during the last five glacial–interglacial cycles. Glob. Planet. Change 75, 119–132.

Stolz, J.F., Chang, S.R., Kirschvink, J.L., 1986. Magnetotactic bacteria and single-domain magnetite in hemipelagic sediments. Nature 321, 849–851.

Tarduno, J.A., Tian, W., Wilkison, S., 1998. Biogeochemical remanent magnetization in pelagic sediments of the western equatorial Pacific Ocean. Geophys. Res. Lett. 25, 3987–3990.

Tauxe, L., 1993. Sedimentary records of relative paleointensity of the geomagnetic field: theory and practice. Rev. Geophys. 31, 319–354.

Tauxe, L., Herbert, T., Shackleton, N.J., Kok, Y.S., 1996. Astronomical calibration of the Matuyama Brunhes Boundary: consequences for magnetic remanence acquisition in marine carbonates and the Asian loess sequences. Earth Planet. Sci. Lett. 140, 133–146.

Tomczak, M., Godfrey, J.S., 1994. Regional Oceanography: An Introduction. Pergamon Press, Oxford.

van der Kaars, S., De Deckker, P., 2002. A Late Quaternary pollen record from deep-sea core Fr10/95, GC17 offshore Cape Range Peninsula, northwestern Western Australia. Rev. Palaeobot. Palynol. 120, 17–39.

Veeh, H.H., McCorkle, D.C., Heggie, D.T., 2000. Glacial/interglacial variations of sedimentation on the West Australian continent margin: constraints from excess ^{230}Th. Mar. Geol. 166, 11–30.

Weeks, R., Laj, C., Endignoux, L., Fuller, M., Roberts, A., Manganne, R., Blanchard, E., Goree, W., 1993. Improvements in long-core measurement techniques: applications in palaeomagnetism and palaeoceanography. Geophys. J. Int. 114, 651–662.

Xuan, C., Channell, J.E.T., 2009. UPmag: MATLAB software for viewing and processing u-channel or other pass-through paleomagnetic data. Geochem. Geophys. Geosyst. 10, Q10Y07, http://dx.doi.org/10.1029/2009GC002584.

Yamazaki, T., 2012. Paleoposition of the Intertropical Convergence Zone in the eastern Pacific inferred from glacial–interglacial changes in terrigenous and biogenic magnetic mineral fractions. Geology 40, 151–154.

Yamazaki, T., Ikehara, M., 2012. Origin of magnetic mineral concentration variation in the Southern Ocean. Paleoceanography 27, PA2206, http://dx.doi.org/10.1029/2011PA002271.